

# First-principles study of electronic structure of $Bi_2Sr_2Ca_2Cu_3O_{10}$

J. A. Camargo-Martínez, Diego Espitia, and R. Baquero  
*Departamento de Física, CINVESTAV-IPN, Av. IPN 2508, 07360 México*  
(Dated: June 28, 2021)

## Abstract

We present for the first time the band structure calculation of  $Bi_2Sr_2Ca_2Cu_3O_{10}$  compound in the tetragonal structure (space group  $I4/mmm$ ). We used the Local Density Approximation (LDA) as in the Wien2k code. We analyze in detail the band structure and the Fermi surface (FS). Our results are in very good agreement with recent experiments. The FS shows the feature known as the Bi-O pocket problem which we associate with the interaction of the O3 atoms with the Cu2-O2 and Bi-O4 planes. Ceramic  $Bi_2Sr_2Ca_2Cu_3O_{10}$  stabilized with Pb has been reported as a superconductor with  $T_c \sim 100$ . CdS microparticles were embedded into the ceramic  $Bi_2Sr_2Ca_2Cu_3O_{10}$ . The composite did show a superconducting phase transition at a lower  $T_c \sim 70K$ . At even lower temperatures re-entrant behavior was observed. The sample regain the superconducting state at  $\sim 47K$  [arXiv:1101.0277 [cond-mat.supr-con]]. This effect is not observe in the ceramic alone. This calculation is useful per ser and also can contribute to a better understanding of this particular re-entrant behavior.

## I. INTRODUCTION

Bismuth cuprates are high-temperature superconductors (HTSC) (except Bi-2201 with  $\sim 2K$ ) with the general formula  $Bi_2Sr_2Ca_{n-1}Cu_nO_y$ . They are normally referred to by the number of  $CuO_2$  planes per unit cell, as Bi-2201, Bi-2212, Bi-2223 and Bi-2234 ( $n = 1, 2, 3$  and  $4$  respectively). Resistivity, susceptibility and magnetization experiments performed on Bi-2212 and Bi-2223 show a transition to the superconducting state at  $\sim 85K$  [1, 2] and  $\sim 110K$  [3, 4] respectively.

The electronic properties of Bi-2212 have been extensively studied both theoretically and experimentally [5–10]. In this work we present a detailed study of the electronic band structure, the density of states and the Fermi surface for Bi-2223. To our knowledge a theoretical study of this compound has not been yet reported in the literature in spite of the fact that the Bi-2223 compound is one of the most suitable HTSC materials for applications [11–13]. Neutron and X-ray diffraction experiments suggest that Bi-2223 presents several orthogonal structures with spacial groups  $Amaa$ ,  $A2aa$  and  $Fmmm$  [14–16] and a tetragonal structure with spatial group  $I4/mmm$  [17, 18]. This structure seems to be more stable when doped with Pb [16–20]. Recently experimental studies of the electronic structure of Bi-2223 by angle-resolved photo-emission spectroscopy (ARPES) have been reported [21–24]. In particular, Ideta et al. [23] report a band splitting at the Fermi surface in the nodal direction associated with the outer and inner  $CuO_2$  planes (OP and IP). We will comment on this point below.

Further, an interesting behavior was observed in a ceramic composite of Bi-2223 embedded with microscopic CdS particles. The ceramic Bi2223 alone becomes superconducting at  $\simeq 100K$  and stays superconducting below this temperature. The composite becomes superconducting at a lower  $T_c \simeq 75K$  and it shows a reentrant behavior [25, 26], i.e., by decreasing the temperature below  $T_c$  the composite returns to the normal state measured by resistivity experiments. Lowering further the temperature the superconducting state reappears. In some systems the normal state is maintained while in others it returns to the superconducting state at a further lower temperature. This phenomenon has been observed since long ago [27]. The disappearance of the superconducting state is, in general, attributed to the formation of a magnetic sub-lattice with a Neel Temperature below the superconducting critical temperature. The re-entrance of the superconducting state is not yet fully understood. The actual composite has the nominal formula  $CdS/Bi_2Sr_2Ca_2Cu_3O_{10}$ . E. Díaz-Valdés et al. [26] reported re-entrant superconductivity in this composite at  $T_c \simeq 47K$ . Our calculation shows no magnetic moment in crystalline  $Bi_2Sr_2Ca_2Cu_3O_{10}$ . We will analyze this case in a further publication.

## II. METHOD OF CALCULATION

The electronic properties for bct  $Bi_2Sr_2Ca_2Cu_3O_{10}$  was determined with the full-potential linearized augmented plane wave method plus local orbital (FLAPW+lo) [28] within the local density approximation (LDA) using the wien2k code [29]. The core states are treated fully relativistically, while for the valence states the scalar relativistic approximation is used. We used a plane-wave cutoff of  $R_{mt}K_{Max} = 8.0$  and for the wave function expansion inside the atomic spheres, a maximum value of the angular momentum of  $l_{max} = 12$  with  $G_{max} = 25$ . We choose a  $17 \times 17 \times 17$  k-space grid which contains 405 points within the irreducible wedge of the Brillouin zone. The muffin-tin sphere radii  $R_{mt}$  (in atomic units) are chosen as 2.3 for Bi, 2.0 for Sr, 1.9 for both Ca and Cu, and 1.5 for O.

## III. THE BI-2223 CRYSTAL STRUCTURE

In this work, we study the Bi-2223 compound with body center tetragonal structure (bct) and space group  $I4/mmm$  ( $D_{4h}^{17}$ ). The structure consists of three Cu-O planes, one Cu1-O1 plane between two Cu2-O2 planes, with Ca atoms between them. Each Cu2-O2 plane is followed by a Sr-O3 and Bi-O4 planes in that order (see Fig. 1). The internal parameters were taken from Ref. [17].

Starting from the experimental parameters, we optimized the  $c/a$  ratio and relaxed the internal coordinates of the structure. In Table I we compare these results with the experimental values reported. The optimized  $c/a$  ratio is 1.56% smaller than the experimental one. In the relaxed structure the Cu1-O1 and Cu2-O2 planes approach each other by  $\sim 0.5\text{\AA}$  while the distance between the Cu2-O2 and Bi-O4 planes increases by  $\sim 0.3\text{\AA}$  as compared to the experimental values. The Sr atoms keep their distance to the Cu2-O2 planes while the O3 atoms move away from the Cu2 ones towards the bismuth atoms.

The main difference between the crystal structure of Bi-2212 [6] and Bi-2223 is the presence of the new  $CuO_2$  plane in the last one labeled in this work as Cu1-O1. The lattice parameter  $a$  is identical in both structures but the  $c$  one differs by  $\sim 7\text{\AA}$ . The presence of the new plane changes the inter-layer distance between neighboring cooper-oxygen

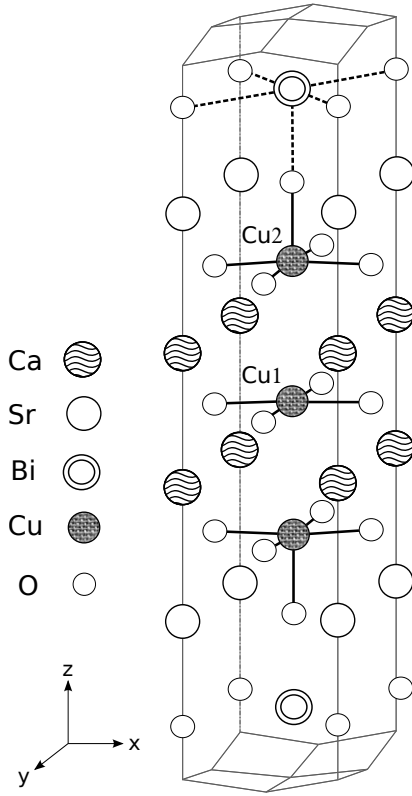


FIG. 1. Primitive cell for body-centered tetragonal  $Bi_2Sr_2Ca_2Cu_3O_{10}$ . O1, O2, O3 and O4 denote oxygens in the Cu1, Cu2, Sr and Bi planes, respectively.

TABLE I. Optimized and relaxed structural parameters of the tetragonal  $Bi_2Sr_2Ca_2Cu_3O_{10}$ . The experimental values were taken from reference [17].

Space group $I4/mmm$ , $z=2$		
	Expt.	This work
$a$	$3.823\text{\AA}$	$3.843\text{\AA}$
$c$	$37.074\text{\AA}$	$36.686\text{\AA}$
$c/a$	9.70	9.55
atom	z	z
Bi	0.2109	0.2072
Sr	0.3557	0.3682
Ca	0.4553	0.4573
Cu1	0.0000	0.0000
Cu2	0.0976	0.0839
O1	0.0000	0.0000
O2	0.0964	0.0847
O3	0.1454	0.1519
O4	0.2890	0.2936

planes. In Bi-2223, the inter-layer  $CuO_2$  distance is  $\sim 0.38\text{\AA}$  larger than in Bi-2212. We will show the contribution in the electronic structure due Cu1-O1 plane.

## IV. RESULTS AND DISCUSSION

### A. Density of states

Fig. 2 shows both the total Density of States (DOS) and the atom-projected densities of states (pDOS). We found that the Fermi level,  $E_F$ , falls in a region of low DOS. This behavior is similar to others Cu-O-based superconductors [30–33]. As might be expected, the Bi-2223 compound maintains the same behavior as the DOS in the Bi-2212 compound [6–9], the only difference is the contribution of new Cu1-O1 plane. The total density of states at  $E_F$ ,  $N(E_F)$ , for Bi-2223 is 3.55 states/(eV cell) which is larger than the one reported for Bi-2212 (2.1–3.3 states/(eV cell)) [6, 8] (see TableII). In the Bi-2223 compound a large contribution comes from the Cu2-O2, Cu1-O1 and Bi-O4 planes. The Bi-O plane contribution creates small electron pockets in the Fermi surface providing conduction electrons. These pockets, nevertheless, do not appear in the experimental results [34]. It is important to note that the new Cu1-O1 plane contributes significantly to  $N(E_F)$ . On the other hand, comparing the atomic contributions to  $N(E_F)$  in both compound (see TableII), we observe a larger contribution of Cu2-O2 planes in Bi-2223 and a similar one from the Bi-O4 planes. The composition at  $E_F$  of the Bi2223 DOS is mainly as follows, Cu2  $d_{x^2-y^2}$ , O2  $p_{x,y}$ , Cu1  $d_{x^2-y^2}$ , O1  $p_{x,y}$ , Bi  $p_{x,y}$ , O4  $p_{x,y}$  and O3  $p_{x,y,z}$  states.

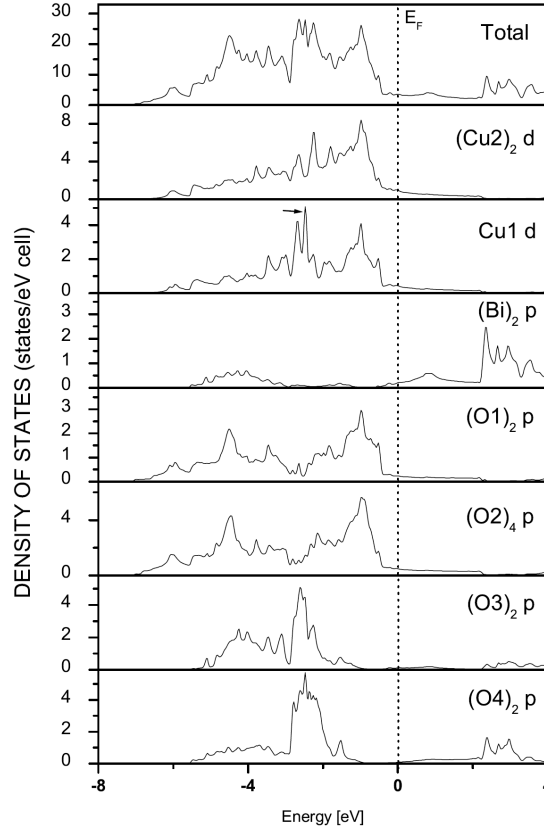


FIG. 2. Total and atom-projected density of states for  $\text{Bi}_2\text{Sr}_2\text{Ca}_2\text{Cu}_3\text{O}_{10}$ . Note the change of scale for each atom contribution. The arrow in the pDOS of Cu1d indicates the peak at 2.49 eV below  $E_F$ .

In Fig. 2 we observe that the contribution of the d-states to the pDOS from the Cu1 and Cu2 atoms is very similar. The only difference is the peak at 2.49 eV below  $E_F$  which corresponds to the contribution of the Cu1  $d_{xz,yz}$  states. The occupied bandwidth of the Cu-O planes is  $\sim 7$  eV. Also observe the wide bandwidth of  $\sim 9$  eV which is typical of the  $dp\sigma$  (bonding and anti-bonding) bands from the two-dimensional  $\text{CuO}_2$  layers [32]. This behavior is similar in the Bi-2212 compound [6–9]. The important contribution to the DOS above  $E_F$  comes mainly from the Bi  $p$  states with a contribution of the O3  $p$  and O4  $p$  states. This oxygen states have a major contribution below at  $E_F$ . The DOS has a minor contribution from both Sr and Ca atoms due to their strong ionic character (Not shown in the Fig. 2 ).

We also calculated the total magnetic moment per cell for Bi-2223 compound and obtained  $0.011 \mu_B$ , whose main

TABLE II. Atomic contributions to the density of states at the Fermi level,  $N(E_F)$ , for both Bi-2212 and Bi-2223. The values are given in units of states/eV-atom. The total  $N(E_F)$  is in units of states/eV cell. The data for Bi-2212 were taken from Ref. [9].

Compound	Atomic state							Total $N(E_F)$
	Cu2 $d$	Cu1 $d$	Bi $p$	O1 $p$	O2 $p$	O3 $p$	O4 $p$	
Bi-2212	-	0.33	0.17	0.16	0.07	0.07	-	2.88
Bi-2223	0.47	0.44	0.10	0.12	0.12	0.06	0.04	3.55

contribution is due to the Cu atoms. This implies that the compound does not exhibit a significant magnetic character at  $T = 0K$ . This fact has implications for the explanation of the re-entrant behavior mentioned above.

## B. Band structure

The band structure of the Bi-2223 compound is shown in the extended zone scheme in Fig.3. (Notice that the  $\bar{M}$  point is the midpoint between the  $\Gamma$  and Z points along the  $\Sigma$  direction). This band structure has many features in common with the Bi-2212 compound [6–9]. In the band structure, the states just below  $E_F$  are primarily Cu2( $3d$ ), O2( $2p$ ), Cu1( $3d$ ) and O1( $2p$ ) states, with a small contribution from Bi( $6p$ ), O4( $2p$ ) and O3( $2p$ ) states. Above  $E_F$ , most of the states are Bi( $6p$ ), O4( $2p$ ) and O3( $2p$ ) with a minor contribution from states from the Cu-O planes. As it can be seen in the Fig.3(A), the band dispersion in the  $\Gamma$ -Z direction (perpendicular to the basal plane) is minimal which means that the bands are strongly two dimensional.

There are five bands crossing at  $E_F$  which are composed primarily of Cu2  $d_{x^2-y^2}$  and O2  $p_{x,y}$  (in red), Cu1  $d_{x^2-y^2}$  and O1  $p_{x,y}$  (in green), Bi  $p_{x,y}$ , O4  $p_{x,y}$  and O3  $p_{x,y}$  (in blue) states in Fig.3 (Color online). The hybridized states from these bands are represented by their respective color mixture and the black line represents the other states. In Table III we present in detail the contribution at  $E_F$  from the different atomic states.

These bands cross  $E_F$  in two regions, the first one between the Z-X(Y- $\Gamma$ ) points and the second one near the  $\bar{M}$  point. In the first region (inset inside Fig.3(A)) there are three nearly degenerate bands, two of them labeled as  $\alpha$  and  $\gamma$ , are composed of Cu1  $d$ , O1  $p$ , Cu2  $d$ , and O2  $p$  states (see Table III). In order to show the character of the  $\alpha$  band at  $E_F$ , we plot in Fig. 4 the corresponding contour plots of the charge density, calculated at  $k = 2\pi(0.19/a, 0.19/b, 0.61/c)$  on the (100) plane cutting the Cu1-O1 and Cu2-O2 bonds. There we see that the Cu-O states are bonding very similar to the corresponding Cu-O states of the Bi-2212 compound [8]. The other band (labeled as  $\beta$ ) is also composed of bonding Cu2  $d$  and O2  $p$  states. These three bands (see inset inside Fig. 3(A)) give the higher contribution to the DOS at the Fermi level.

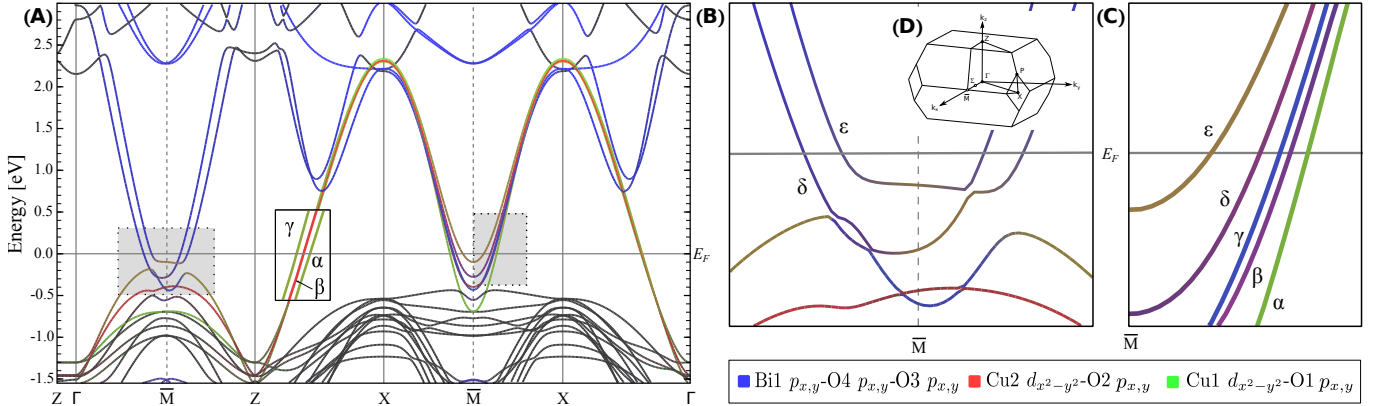
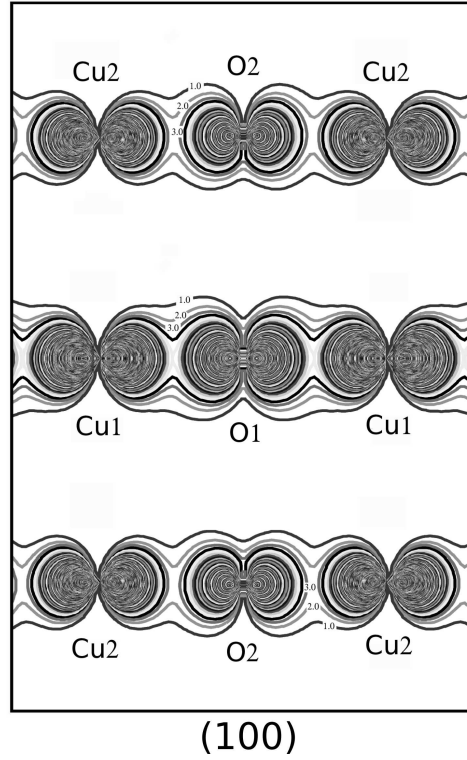


FIG. 3. (Color online) The band structure of the  $Bi_2Sr_2Ca_2Cu_3O_{10}$  compound in the extended zone scheme. Note that the behavior of the bands are similar along the X-Z and the X- $\Gamma$  directions. The shaded areas in the figure (A) are amplified in Figures (B) and (C) respectively. In (D) we show the first Brillouin zone for a body-centered tetragonal structure for completeness.

In the second region (near the  $\bar{M}$  point), the behavior of the bands are different along the  $\Gamma$ -Z and the X-Y directions (see shaded areas in Fig. 3(A)). Further, as seen in Fig. 3(B) there are two bands, labeled as  $\delta$  and  $\varepsilon$ , crossing at  $E_F$  in the  $\Sigma$  direction, which are non symmetric around the  $\bar{M}$  point. Between the  $\Gamma$  and Z points, the  $\delta$  band is

TABLE III. Detailed contribution from the different atomic states to the bands at  $E_F$ .

Direction	Band	Bi	O4	O3	Cu1	O1	Cu2		O2
		$p_{x,y}$	$p_{x,y}$	$p_{x,y,z}$	$d_{x^2-y^2}$	$p_{x,y}$	$d_{x^2-y^2}$	$d_{z^2}$	$p_{x,y}$
Z-X	$\alpha$	-	-	-	29%	25%	29%	-	17%
	$\beta$	-	-	-	-	-	62%	-	38%
	$\gamma$	-	-	-	28%	24%	29%	-	19%
$\Gamma$ -Z ( $\Sigma$ )	$\delta$	44%	24%	25%	-	-	4%	-	3%
$\Gamma$ - $\bar{M}$	$\varepsilon$	33%	9%	19%	6%	3%	16%	6%	8%
$\bar{M}$ -Z	$\varepsilon$	47%	13%	27%	-	-	6%	-	11%
$\bar{M}$ -Y(X)	$\alpha$	-	-	-	44%	16%	29%	-	11%
	$\beta$	18%	12%	8%	-	-	45%	-	17%
	$\gamma$	42%	25%	19%	10%	4%	-	-	-
	$\delta$	17%	7%	11%	-	-	47%	-	18%
	$\varepsilon$	-	-	-	24%	8%	46%	7%	15%


 FIG. 4. Charge density contour plots for the  $\alpha$  band at  $E_F$  in the Z-X direction, on the (100) plane cutting the Cu1-O1 and Cu2-O2 bonds. Contours are given on a linear scale which values are  $10^{-3}e/a.u.^3$ .

composed of weakly bonding Bi  $p$ -O4  $p$  and anti-bonding Bi  $p$ -O3  $p$  states. The  $\varepsilon$  band between the  $\Gamma$  and  $\bar{M}$  points, is formed of anti-bonding Bi  $p$ -O4  $p$  and Bi  $p$ -O3  $p$  states and hybridizes with Cu2  $d$ -O2  $p$  and Cu1  $d$ -O1  $p$  states, with a small contribution from Cu2  $d_{z^2}$  states, while between the  $\bar{M}$  and Z points it is composed of anti-bonding Bi  $p$ -O4  $p$  states and hybridizes with Cu2  $d$ -O2  $p$  and O3  $p$  states. In Fig. 5 we show the contour plots of the charge density in the (100) and (110) planes, cutting the Bi-O and Cu-O bonds corresponding to the band  $\varepsilon$  in Fig. 3(B) at  $k = 2\pi(0.42/a, 0, 0)$ , very close to  $E_F$ . Fig. 5(A) shows the strong Bi-Bi bonding character ( $pp\sigma$ ) and the anti-bonding character of the Cu-O planes. In Fig. 5(B) we show the contour plot of the charge density on the (110) plane. There we can see the anti-bonding character of the Bi-O and Cu2-O3 states. This behavior is similar to the one reported for Bi-2212 by Massidda et al. [8].

Around the  $\bar{M}$  point but in the X-Z direction (see Fig.3(C)), the  $\alpha$ ,  $\beta$ ,  $\gamma$ ,  $\delta$  and  $\varepsilon$  bands have a different character. The band  $\alpha$  is a combination of bonding Cu1  $d$ -O1  $p$  and Cu2  $d$ -O2  $p$  states (see TableIII). The bands  $\beta$  and  $\delta$  are

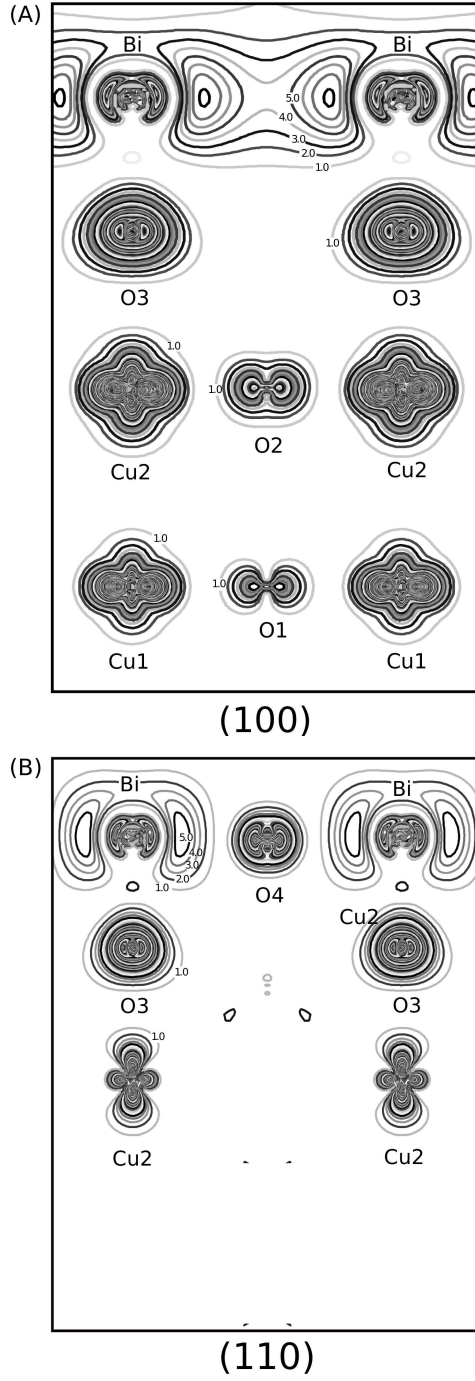


FIG. 5. Charge density contour plots for the  $\varepsilon$  band at  $E_F$  in  $\Gamma$ - $\bar{M}$  direction, in the (100) and (110) planes. Note the bonding character of Bi-Bi bonds and the antibonding character of Cu-O bonds in (100) plane. In (110) plane the contribution of the Cu1-O1 plane is not observed (see text). Contours are given as in Fig. 4.

composed of hybrids of bonding Cu2  $d$ -O2  $p$ , antibonding Bi  $p$ -O4  $p$  and Bi  $p$ -O3  $p$  states. The band  $\gamma$  is composed of weakly bonding Bi  $p$ -O4 and Bi  $p$ -O3  $p$  states, and hybridizes with antibonding Cu1  $d$ -O1  $p$  states. Finally, the band  $\varepsilon$  has a similar behavior as the band  $\alpha$  but with a small contributions of the Cu2  $d_{z^2}$  state at  $E_F$  (see Table III).

In the Fig.3(A), the copper-oxygen bands that cross at  $E_F$  extend from 1.5 eV below to 2.3 eV above  $E_F$ . These bands have their maximum energy at the X point, and their minimal energy at the Z point and are anti-bonding. These bands present a strong Cu-O  $dp\sigma$  character. Around the  $\bar{M}$  point, the Bi-O bands extend to about 0.57 eV below  $E_F$  and hybridize with Cu2  $d_{x^2-y^2}$ -O2  $p_y$  states. The Bi-O bands presents a  $pp\sigma$  character. The contribution



of the Bi-O states at  $E_F$  are due to the interaction with the O3 and the Cu2-O2 planes. The Bismuth bands present an interesting feature around  $\Gamma$  and Z. Exactly at those points, the band derives from only  $p_z$  state, while around those points the band derives from combinations of all  $p$  states.

The bands around the X(Y) point are  $\sim 0.54$  eV below  $E_F$  while in the Bi-2212 compound this bands lie about  $\sim 0.1$  eV below  $E_F$  [6–9]. These bands are primarily antibonding Cu1  $d_{xz,yz}$ -O1  $p_z$  and Cu2  $d_{xz,yz}$ -O2  $p_z$  states with a  $pp\pi$  character. Taking the band structures of  $Bi_2Sr_2Ca_{n-1}Cu_nO_y$  compounds with  $n = 1$  and 2, calculated by Sterne and Wang [10] and comparing with our calculation ( $n = 3$ ), we observed that the number of bands crossing at  $E_F$  in  $\Gamma$ -X direction is proportional to the number of Cu-O planes. A similar idea had been outlined by Mori et al. [36]. We also noted that the energy below  $E_F$  of the Bi-O bands around  $\bar{M}$  point is deeper proportionally to the number of Cu-O planes.

### C. Fermi surface

In Fig.6 we show the Fermi Surface (FS) of the Bi-2223 compound in an extended zone scheme. This FS has in general the same behavior to the one reported for the Bi-2212 compound, with the similar highly anisotropic low-dimensionality [8, 9, 37]. Our calculation presents two additional surfaces. Around the X(Y) there are three not quite degenerate hole surfaces labeled as  $\alpha$ ,  $\beta$  and  $\gamma$  (corresponding to the respective bands in Fig.3). In  $\Gamma$ -X and equivalent directions, the  $\alpha$  and  $\gamma$  surfaces consists of hybrids of Cu1-O1 and Cu2-O2 states and the  $\beta$  surface is composed of Cu2-O2 states. The  $\alpha$  and the  $\beta$  surfaces are close to be rounded squares. As we approach from the X(Y) to the  $\bar{M}$  point, the  $\beta$  and the  $\gamma$  surfaces get an additional contribution from Bi-O4 states (see Table III). As we can see from Fig.6 the  $\alpha$  surface has more nesting than  $\beta$  and  $\gamma$  surfaces.

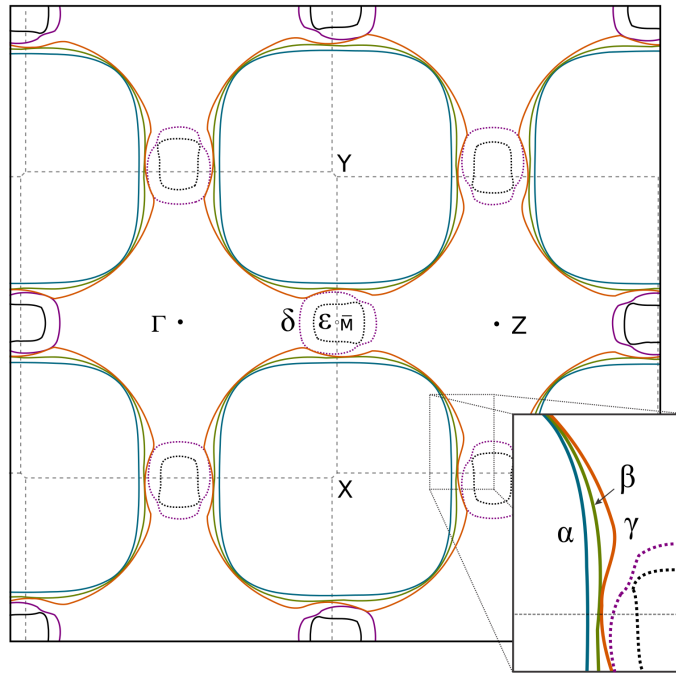


FIG. 6. (Color online) Fermi Surface at  $k_z = 0$  of  $Bi_2Sr_2Ca_2Cu_3O_{10}$  in an extended zone scheme. The Bi-O pockets are represented by violet and black lines (dashed lines).

The FS of Bi-2223 calculated by ARPES is shown in ref. [23]. In that work they found two surfaces on the  $\Gamma$ -X(Y) direction (see Fig.7), that they call outer copper planes (OP) and inner copper plane (IP) and suggest the possibility that OP's are degenerate. The full width at half maximum (FWHM) of the momentum distribution curve (ARPES resolution) for the OP is  $\sim 0.011\text{\AA}$  and the IP is  $\sim 0.0074\text{\AA}$ , at  $E_F$ . Other experimental work with the same technique [21, 22] does not report this band splitting.

We identified these IP and OP as  $\alpha$  and  $\beta$ ,  $\gamma$  surfaces respectively in our FS. On  $\Gamma$ -X direction we calculated the differences in momentum  $\Delta|k|_{OP-IP}$  and  $\Delta|k|_{OP-OP}$  (see Fig.7) and found  $\sim 0.005\text{\AA}$  and  $\sim 0.01\text{\AA}$  respectively. Comparing these differences with the ARPES resolution in the work just mentioned, it is clear that it cannot resolve the existence of the three bands separately. Our results support the idea that the IP is composed of Cu2-O2 states,



and the OP's are composed of hybrids from Cu1-O1 and Cu2-O2 states.

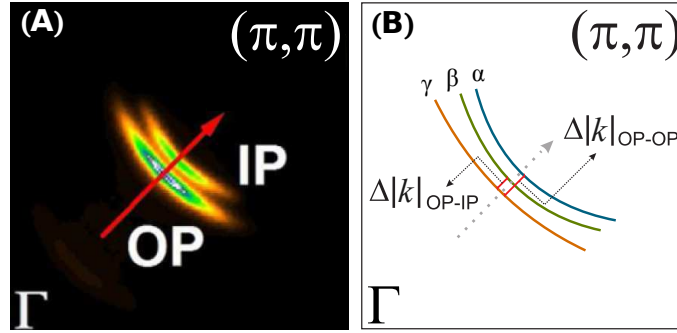


FIG. 7. (Color online) (A) The Fermi surface (FS) of Bi-2223 calculated by ARPES [23] in the nodal direction. (B) Schematic FS showing the band splitting and the  $\Delta|k|$  calculated in this work.

Now, around the  $\bar{M}$  point we observe two surfaces (Bi-O pockets) in comparison with the single surface observed in the Bi-2212 compound. These surfaces, labeled as  $\delta$  and  $\varepsilon$  (see Fig. 6) form small closed electron surfaces. The  $\delta$  surface is close to be a rounded square with a small convexity pointing towards Z point, while  $\varepsilon$  surface is almost a rounded rectangle. In the experimental reports the Bi-O planes show always a nonmetallic character [34]. In the theoretical calculations this is called the “Bi-O pocket problem”.

Finally, around  $\Gamma$  and Z points there are electron surfaces that look like a between them, this characteristic is due to highly two-dimensionality of the system, however from the band structure and the FS of the Bi-2223 compound we observe less two dimensional behavior than the reported for the Bi-2212 compound [8, 9].

## V. CONCLUSIONS

We presented here a detailed analysis of the electronic properties of the tetragonal ( $I4/mmm$ ) Bi-2223 compound. To the best of our knowledge there is no previous theoretical calculation for this compound. Our calculation was done using the Full-potential linearized augmented plane wave method plus Local orbitals within the Local density approximation using Wien2k code.

We studied the contribution of the Cu1-O1 plane to the electronic properties of the Bi-2223 compound. This plane has an important contribution to the DOS at the  $E_F$  (0.56 states/eV-atom) which is similar to the one of the Cu2-O2 plane. Compared to Bi-2212 [9], Bi-2223 presents a higher DOS at  $E_F$ . This is due to the new Cu-O plane.

Our calculated band structure present Bi-O bands at the  $E_F$ . This so called Bi-O pocket problem is in disagreement with the experimental results. This problem also appears in the theoretical calculations concerning Bi-2212 and Bi-2201. Taking the band structures of Bi-2212 and Bi-2201 [10] and comparing with our calculation (Bi-2223), we observed that the number of bands crossing at  $E_F$  in  $\Gamma$ -X direction is proportional to the number of Cu-O planes. This is in agreement with the idea outlined by Mori et al. [36]. We also noted that the energy below  $E_F$  of the Bi-O bands around  $\bar{M}$  point is deeper proportionally to the number of Cu-O planes.

The Fermi surface (FS) calculated in this work presents a good agreement with the experimental result calculated, in the nodal direction, by angle-resolved photo-emission spectroscopy (ARPES) [23].

Our work is useful per se and contributes to the understanding of the re-entrant behavior found in the ceramic composite of  $CdS/Bi_2Sr_2Ca_2Cu_3O_{10}$ .

## VI. ACKNOWLEDGMENTS

The authors acknowledge to the GENERAL COORDINATION OF INFORMATION AND COMMUNICATIONS TECHNOLOGIES (CGSTIC) at CINVESTAV for providing HPC resources on the Hybrid Cluster Supercomputer “Xihucoatl”, that have contributed to the research results reported within this paper.

---

[1] S. A. Sunshine et al., *Phys. Rev. B* **38**, 893 (1988).

- [2] A. Maeda, M. Hase, I. Tsukada, K. Noda, S. Takebayashi, and K. Uchinokura, *Phys. Rev. B* **41**, 6418 (1990).
- [3] J. L. Tallon, R. G. Buckley, P. W. Gilberd, M. R. Presland, I. W. M. Brown, M. E. Bowden, L. A. Chistian and R. Goguel, *Nature* **333**, 153 (1988).
- [4] J. M. Tarascon, W. R. McKinnon, P. Barboux, D. M. Hwang, B. G. Bagley, L. H. Greene, G. W. Hull, Y. LePage, N. Stoffel and M. Giroud, *Phys. Rev. B* **38**, 8885 (1988).
- [5] P.V. Bogdanov et al., *Phys. Rev. B* **64**, 180505 (2001) an references there in.
- [6] M. S. Hybertsen and L. F. Mattheiss, *Phys. Rev. Lett.* **60**, 1661 (1988).
- [7] L. F. Mattheiss and D. R. Hamann, *Phys. Rev. B* **38**, 5012 (1988).
- [8] S. Massidda, J. Yu and A. J. Freeman, *Phys. C* **152**, 251 (1988).
- [9] H. Krakauer and W. E. Pickett, *Phys. Rev. Lett.* **60**, 1665 (1988).
- [10] P. A. Sterne and C. S. Wang, *J. Phys. C: Solid State Phys.* **21**, L949 (1988).
- [11] Kitaguchi H and Kumakura H. *MRS Bulletin: Advances in Bi-Based High-Tc Superconducting Tapes and Wires* **26**, 121 (2001).
- [12] T. J. Arndt, A. Aubele, H. Krauth, M. Munz, B. Sailer, and A. Szulczyk, *IEEE Transactions on Applied Superconductivity* **13**, 3030 (2003).
- [13] W. Hassenzahl, et al. *Electric power applications of superconductivity. Proceedings of the IEEE. Special Issue on Applications of Superconductivity* **92(10)**, 1655 (2004).
- [14] V. F. Shamray, A. B. Mikhailova, and A. V. Mitin, *Crystallography Reports* **54**, 584 (2009).
- [15] A. Sequeira A, J.V. Yakhmi, R.M. Iyer, H. Rajagopal and P.V.P.S.S. Sastry, *Physica C* **167**, 291 (1990).
- [16] W. Carrillo-Cabrera and W. Gopel, *Phys. C* **161**, 373 (1989).
- [17] X. Zhu, S. Feng, J. Zhang, G. Lu, K. Chen, K. Wu, Z. Gan, *Modern Phys. Lett. B* **3**, 707 (1989).
- [18] J. Yang, C. Ye, B. Zhang, J. Li, J. Kang, Y. Ding, Y. He, J. Zhang, A. He, J. Xiang, *Modern Physics Letters B* **4**, 791 (1990).
- [19] G. Miede, T. Vogt, H. Fuess and M. Wilhelm, *Phys. C* **171**, 339 (1990).
- [20] E. Giannini, R. Gladyshevskii, N. Clayton, N. Musolino, V. Garnier, A. Piriou, R. Flukiger, *Current Applied Physics* **8**, 115 (2008).
- [21] D. L. Feng et al., *Phys. Rev. Lett.* **88**, 107001 (2002).
- [22] H. Matsui et. al., *Phys. Rev. B* **67**, 060501 (2003).
- [23] S. Ideta et al., *Phys. Rev. Lett.* **104**, 227001 (2010).
- [24] S. Ideta et al., *Phys. C Lett.* **470**, S14 (2010).
- [25] Y. Zhao, G. D. Gu, G. J. Russell, N. Nakamura, S. Tajima, J. G. Wen, K. Uehara, and N. Koshizuka, *Phys. Rev. B* **51**, 3134 (1995).
- [26] E. Díaz-Valdés, G. S. Contreras-Puente, N. Campos-Rivera, C. Falcony-Guajardo and R. Baquero, *arXiv:1101.0277* [cond-mat.supr-con].
- [27] H. Eisaki, H. Takagi, R. J. Cava, B. Batlogg, J. J. Krajewski, W. F. Peck, Jr., K. Mizuhashi, J. O. Lee, and S. Uchida, *Phys. Rev. B* **50**, 647 1994.
- [28] O. K. Andersen, *Phys.Rev.B* **12**, 3060 (1975).
- [29] P. Blaha, K. Schwars, G.K.H. Madsen, D. Kvasnicka, and J. Luitz, *WIEN2K:Full Potential-Linearized Augmented Plane waves and Local Orbital Programs for Calculating Crystal Properties*, edited by K. Schwars, Vienna University of Technology, Austria, (2001).
- [30] L. F. Mattheiss, *Phys. Rev. Lett.* **58**, 1028 (1987).
- [31] L. F. Mattheiss and D. R. Hamann, *Solid State Commun.* **63**, 395 (1987).
- [32] S. Massidda, J. Yu, A. J. Freeman, and D. D. Koelling, *Phys. Lett. A* **122**, 198 (1987).
- [33] D. R. Hamann and L. F. Mattheiss, *Phys. Rev. B* **38**, 5138 (1988).
- [34] M. Tanaka et al., *Nature* **339**, 691 (1989).
- [35] A. Damascelli et al., *Rev. Mod. Phys.* **75**, 473 (2003).
- [36] M. Mori, T. Tohyama, and S. Maekawa, *Phys. Rev. B* **66**, 064502 (2002).
- [37] V. Bellini, F. Manghi, T. Thonhauser and C. Ambrosch-Draxl, *Phys.Rev.B* **69**, 184508 (2004).